JOURNAL OF MATERIALS SCIENCE 27 (1992) 983–989

Small-punch and TEM-disc testing techniques and their application to characterization of radiation damage

J. KAMEDA
Ames Laboratory, Iowa State University, Ames, IA 50011, USA
X. MAO
Department of Mechanical Engineering, The University of Calgary, Calgary, Alberta, Canada T2N 1N4

The present paper summarizes the development of miniaturized small-punch (SP) and TEM-disc (TD) testing techniques and shows their applicability in characterizing the mechanical properties of irradiated materials. The yield strength, ductility and fracture toughness, J_{Ic}, were empirically estimated by analysing the deformation and fracture behaviour observed in the miniaturized specimen tests. The ductile–brittle transition temperature (DBTT) was determined from the variation of the SP or TD fracture energy with temperature. A linear correlation between the DBTT obtained from the SP and Charpy V-notched specimen tests has been theoretically and experimentally established. The problems of cracking detection and data scattering often observed in the SP or TD specimen tests are discussed in terms of heterogeneous embrittlement behaviour of materials. It has been demonstrated that these miniaturized testing techniques are capable of evaluating hardening, DBTT shifts and J_{Ic} decreases caused by neutron irradiation.

1. Introduction

Neutron irradiation produces degradation of the mechanical properties of alloys. For example, microstructure evolution and solute segregation, resulting from the dynamic interaction between dislocations or solute and defect clusters during irradiation, facilitates the formation of microvoids and hardening, and gives rise to an increase in the ductile–brittle transition temperature (DBTT) [1]. The characterization of the mechanical properties change induced by irradiation is essentially required for developing new materials for future fusion nuclear energy systems and maintaining the safety margin of currently operating fission nuclear reactor components. However, it is generally difficult to apply conventional mechanical testing methods to study irradiated materials. There are three principal reasons for developing miniaturized testing techniques: (1) irradiation testing facilities can be most efficiently utilized when small-size specimens are used; (2) simulation experiments of fusion irradiation conditions are only made on a small scale; (3) handling of small radioactive samples is a much greater advantage over that of large ones. Moreover, miniaturized mechanical testing methods are useful for evaluating more readily the toughness deterioration of structural materials caused by the exposure to high temperatures or aggressive environments, such as temper embrittlement and stress corrosion cracking of turbine rotor steels [2].

While Lucas [3] recently has reviewed a variety of miniaturized testing techniques, the present paper attempts to focus on a recent progress on the development of miniaturized small-punch (SP) and TEM-disc (TD) testing techniques and to demonstrate their applicability to the characterization of radiation damage.

2. Small-punch and TEM-disc testing techniques

The materials used in this work were a variety of ferritic and austenitic steels with different yield strengths, grain sizes and impurities, and iron and Cu–Be alloys. The chemical compositions, and the deformation and fracture properties obtained using conventional mechanical testing methods are presented elsewhere in detail [4–12].

SP specimens (10 mm × 10 mm × 0.5 or 0.25 mm) and TD specimens (3 mm diameter × 0.25 mm) were prepared from the heat-treated materials or the undamaged portion of broken Charpy V-notched (CVN) bars. The SP and TD specimens were mechanically polished using 600–1500 grid emery papers and some of the specimens were further polished using 0.5 μm alumina powders.

The punch, ball-punch tip and specimen holder designed for SP and TD tests are shown in Fig. 1 [5, 13]. The SP and TD holders consist of an upper and lower die and four clamping screws. When an SP or TD specimen was placed in the holder, a slight clearance between the bottom surface of the upper die and the top surface of the specimens was provided to

0022–2461

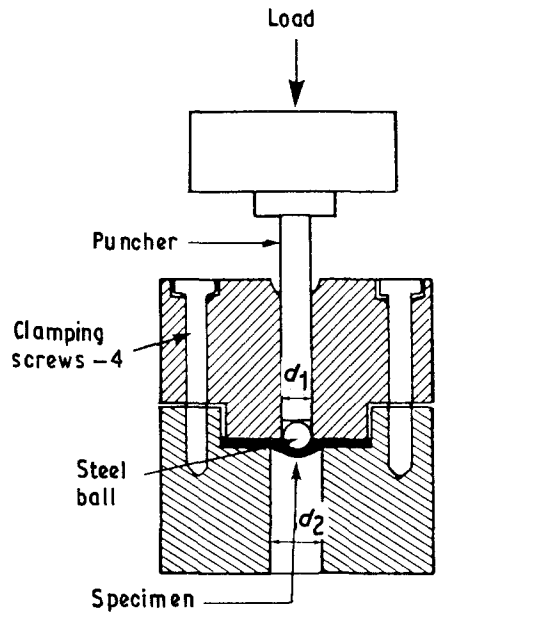

Figure 1 Loading and specimen support configurations, and geometry of SP and TD specimens.

maintain a stress-free state prior to loading. This clamping holder enabled us to prevent specimens from cupping upwards during punching and therefore the deformation was concentrated in the region below the punch. The bore diameter of the lower die was designed such that the deformed specimens were not subjected to frictional forces arising from contact of the SP or TD specimen with the inner wall of the lower die hole.

All the SP and TD tests were performed on an universal testing machine over a wide temperature range (77–475 K) with special attention to maintaining an accurate loading alignment. Test temperatures were achieved using a mixture of isopentane and liquid nitrogen or heated silicone oil. The SP and TD tests were performed at a crosshead speed of $2.0–3.3 \times 10^{-2}$ mm s^{-1}.

Fig. 2 illustrates schematically a load versus deflection curve obtained from the SP and TD tests. We can see four deformation regimes: (I) elastic bending, (II) plastic bending, (III) membrane stretching, and (IV) plastic instability [5, 14, 15]. Note that fracture occurs in

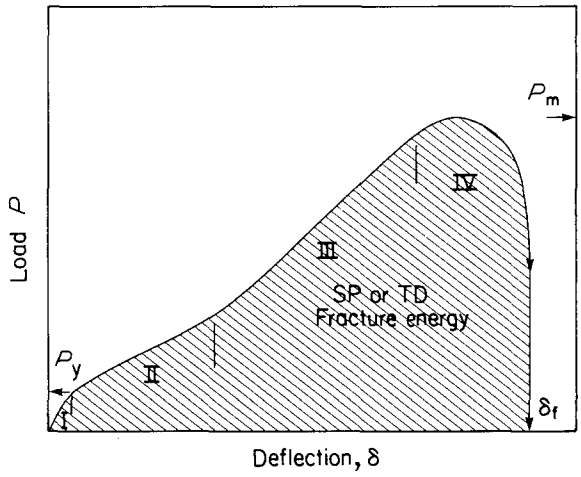

Figure 2 Schematic illustration of load versus deflection curve obtained from SP and TD tests indicating the four deformation regimes and several parameters representing the deformation and fracture properties. I, Elastic bending; II, plastic bending; III, membrane bending; IV, plastic instability.

the different regimes depending on the toughness of materials. From the load versus deflection curve, several parameters (i.e. the yielding load, P_y, the maximum load, P_m, the fracture deflection, δ_f, and the SP or TD fracture energy) are determined to characterize the deformation and fracture properties of materials. In order to investigate the radial distribution of plastic strain, the measurement of a change in the thickness and the application of a recrystallization etch method were made at the mid-section of load-interrupted and fractured specimens [4, 5]. In the following sections, we demonstrate how the parameters obtained from the SP and TD tests are analysed to characterize the mechanical properties of nonirradiated and irradiated materials.

3. Ductility and fracture toughness

Fig. 3 depicts a linear relationship between the yield strength, σ_y, and P_y/t_0^2 measured from the SP and TD tests for various strength materials [5]. The empirical

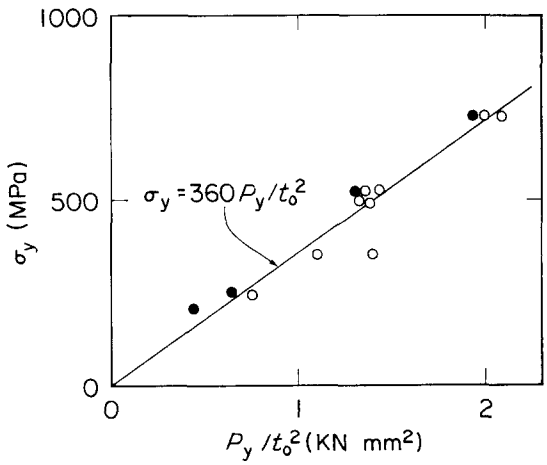

Figure 3 Relationship between yield strength and P_y/t_0^2 obtained from (○) SP and (●) TD tests of various materials.

relation is given by

$$\sigma_y(\text{MPa}) = 360 P_y/t_0^2(\text{kN mm}^{-2}) \quad (1)$$

where t_0 is the initial specimen thickness. However, the plot of the ultimate strength against P_m/t_0^2 did not show a unique relationship. This is probably because the specimen thickness substantially decreases in the plastic instability regime.

An attempt was made to analyse the deformation behaviour observed in the miniaturized specimens using a semi-analytical membrane stretching theory and the recrystallization etch method [4, 5]. It was found that the radial distribution of plastic strain determined from the measurement of the thickness change is in close agreement with that found by the recrystallization etch method. Thus, the equivalent plastic strain, ε_q, is the same as the thickness strain, and is given by

$$\varepsilon_q = \ln(t_0/t) \quad (2)$$

where t is the thickness of the deformed specimen. The maximum thinning of deformed SP and TD specimens was observed along a circular plane inclined from the loading axis by about 45° solid angle and ductile fracture mostly occurred there. Because the thickness measurement of the axisymmetrically deformed SP and TD specimens and the use of the recrystallization etch method are impractical, it is reasonable to make an estimate of the plastic strain from the deflection measured in the SP and TD tests. Fig. 4 indicates a logarithmic relationship between ε_q and δ/t_0 for both the SP and TD tests of various materials. Although data scattering occurred significantly more in the TD specimen test than in the SP specimen test, the empirical equation can be given by

$$\varepsilon_q = 0.12(\delta/t_0)^{1.72} \qquad \varepsilon_q > 0.05 \quad (3)$$

This equation is somewhat different from those originally proposed which were given for the SP and TD tests, respectively, for $\varepsilon_q > 0.01$ [5]. Using Equation 3, the fracture strain, ε_{qf}, can be estimated from δ_f. It has been shown [4, 5] that the estimated fracture strain does not depend on the initial thickness and type of specimens.

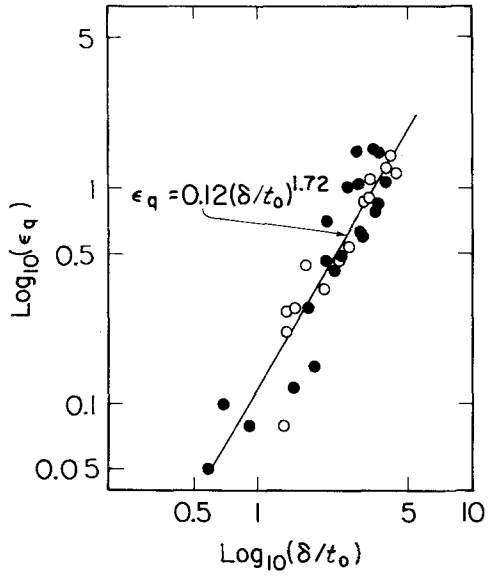

Figure 4 Logarithmic relationship between plastic strain and δ/t_0 obtained from (○) SP and (●) TD tests of various materials.

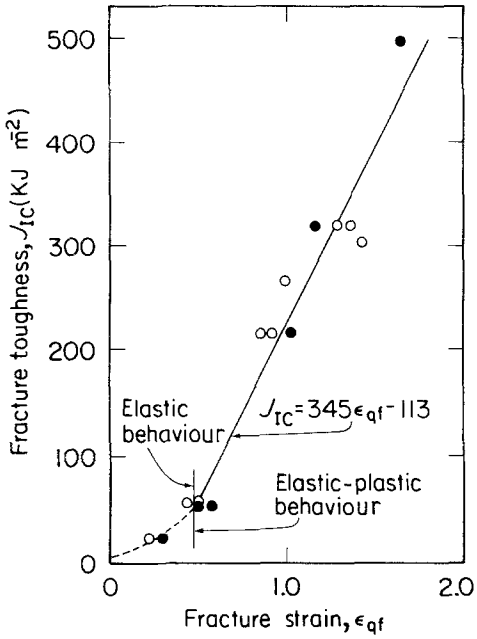

Figure 5 Relationship between fracture strain and fracture toughness obtained from (○) SP and (●) TD tests of various materials.

While the fracture strain represents a relative measure of the ductility, the fracture toughness, J_{Ic}, provides the resistance to the ductile crack initiation which is an important parameter for characterizing structural materials. The measurement of the vaid J_{Ic} value requires the use of large specimens, which is not appropriate for irradiated materials. Therefore, it is important to establish a fracture strain versus fracture toughness relation. Fig. 5 depicts the plot of J_{Ic} measured from compact tension (CT) specimen tests against ε_{qf} determined from the SP and TD tests for different strength materials [5, 12]. This empirical relation qualitatively agreed with one predicted by Bayoumi and Bassim [16]. J_{Ic} is proportionately related to $(\varepsilon_{qf})^2$ and ε_{qf} in the elastic and elastic–plastic regimes, respectively. For the case of $\varepsilon_{qf} > 0.4$, J_{Ic} is given by

$$J_{Ic} = 345\varepsilon_{qf} - 113 \quad (\text{kJ m}^{-2}) \quad (4)$$

It is interesting to note that the relation does not depend on the yield strength in the range from 250–730 MPa.

4. Determination of ductile–brittle transition temperature

The degree of radiation damage in bcc metals and alloys is often characterized in terms of an increase in the DBTT. Fig. 6 shows the variation of SP fracture energy with temperature, together with the morphology of plastic bulging and crack propagation [13]. The SP specimen test clearly demonstrated the ductile–brittle fracture mode transition behaviour. At a lower temperature range, brittle cracks propagated

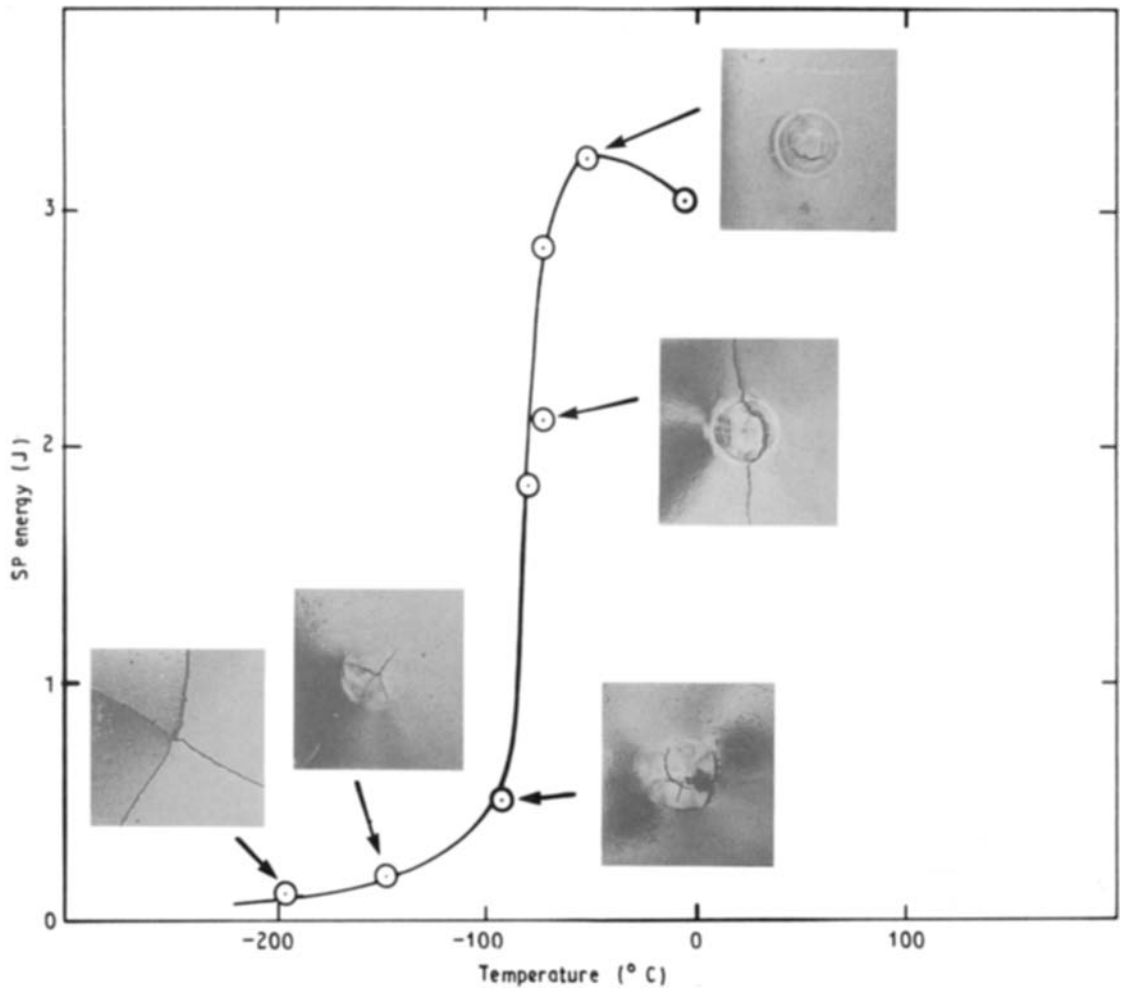

Figure 6 Ductile–brittle fracture mode transition behaviour observed in SP specimen tests of Ni–Cr steel doped with tin.

along the radial direction. With increasing temperature, the plastic bulging proceeded and ductile cracks propagated circumferentially in the heavily stretched part. Similar behaviour was observed in the TD specimen test [17]. It is clear that the DBTT can be defined from the SP and TD tests. However, there are several important factors which must be considered in determining the DBTT from the SP and TD tests.

First, a substantially lower DBTT was obtained from the SP and DT tests than from the CVN test [13, 17]. This difference is ascribed to the fact that SP or TD specimens are deformed using static loading and under the biaxial stress state, which are less severe conditions for brittle fracture. Thus it is necessary to establish a correlation between $(DBTT)_{SP}$ and $(DBTT)_{CVN}$. For this purpose, a kinetic model for the ductile–brittle fracture mode transition behaviour has been developed [18]. In this model, it is assumed that in the DBTT range, ductile and brittle fracture can be characterized in terms of the thermally activated crack growth in shear and tension, respectively. The fracture probability can be represented by the product of the bond-breaking rate, the process volume, V, and the density of crack nuclei, F. Moreover, the dislocation behaviour near the tip of a crack is considered to be thermally activated under the applied strain rate, $\dot{\varepsilon}$. At the DBTT, both the ductile and brittle fracture probabilities are the same. Therefore, the DBTT can be given by the thermal activation energy term characterizing the bond-breaking and dislocation behaviour and the parameters related to mechanical and microstructural factors (F, V and $\dot{\varepsilon}$). Because the intrinsic fracture properties (i.e. the activation energy term) are not affected by testing conditions and methods, the correlation of the DBTT between the SP and CVN testing techniques is given by

$$(DBTT)_{SP} = \left\{ \ln\left[\left(\frac{V_s F_s}{V_t F_t} \right) \left(\frac{\dot{\varepsilon}_0}{\dot{\varepsilon}} \right)^2 \right]_{CVN} \Big/ \ln\left[\left(\frac{V_s F_s}{V_t F_t} \right) \left(\frac{\dot{\varepsilon}_0}{\dot{\varepsilon}} \right)^2 \right]_{SP} \right\} (DBTT)_{CVN} = \alpha (DBTT)_{CVN} \quad (5)$$

where $\dot{\varepsilon}_0$ is the parameter related to the dynamic material properties, and the subscripts s and t indicate shear and tension. It is apparent from Equation 5 that increasing applied strain rate is most likely to cause $(DBTT)_{SP}$ to become close to $(DBTT)_{CVN}$. Fig. 7 shows the relationship between the DBTTs experimentally determined for various Ni–Cr, Cr–Mo–V and HT-9 steel with different yield strengths, and types and quantities of impurities [6–8, 11, 13, 17–19]. Although there is some scattering due to the microstructure difference, a linear correlation exists which is consistent with that predicted by the kinetic theory.

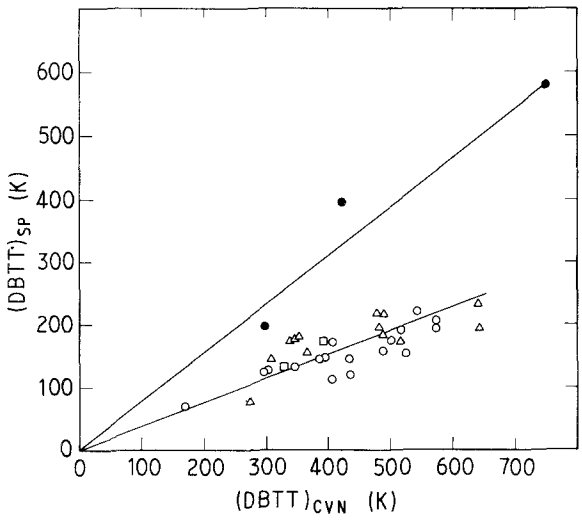

Figure 7 Correlation between $(DBTT)_{SP}$ and $(DBTT)_{CVN}$ for (○) Ni–Cr steel, undoped, or doped with phosphorus or tin, (●) Ni–Cr steel doped with antimony, (△) Cr–Mo-V steel, (□) HT-9 steel.

The empirically determined value of α is about 0.4 for all the steel but the antimony-doped Ni–Cr steel. The different DBTT relation observed for the antimony-doped steel is probably due to the remarkably strong and heterogeneous embrittlement effect of antimony [7].

The second problem is the detection of cracking which becomes important in determining the SP or TD fracture energy and thereby the DBTT. Serration was observed in the load versus deflection curve from the SP test of temper-embrittled materials [19]. The occurrence of serrations was found to arise from discrete crack propagation. It has been shown that when cracks discretely propagate under punch loading, the macroscopic load drop is reflected by the extensive opening of propagating cracks. Therefore, in this case it is more reasonable to define the SP or TD fracture energy at the initiation of serrations than at the stage of distinct load drop.

Finally, it has been shown [14, 17, 19] that considerable scattering of the SP or TD fracture energy is frequently observed in the DBTT range. For example, with increasing grain size or heterogeneity of segregated impurities, the ductile–brittle fracture mode transition appeared in a wider temperature range [14, 19]. The data scattering is a statistical problem associated with miniaturized testing methods. Because in the SP and TD tests only small volumes of the grain matrix or a few grain boundaries are stressed during punch loading, the heterogeneous fracture behaviour significantly emerges as data scattering. Taking a number of data is not realistic for evaluating irradiated materials. In order to deal with the data scattering, Misawa *et al.* [17] applied Weibull extreme statistics. Then the use of the statistical theory makes it possible to estimate the lower bound of DBTT from a considerably smaller number of the SP or TD specimen tests.

5. Application of SP and TD testing techniques in evaluating radiation damage

It is apparent from the previous sections that the SP and TD testing methods are suitable tools for examining irradiated materials because of their ability to make a reasonable estimate of the yield strength, J_{Ic} and DBTT. We now attempt to evaluate neutron irradiation-induced hardening and embrittlement in iron alloys and ferritic steel using the miniaturized testing techniques.

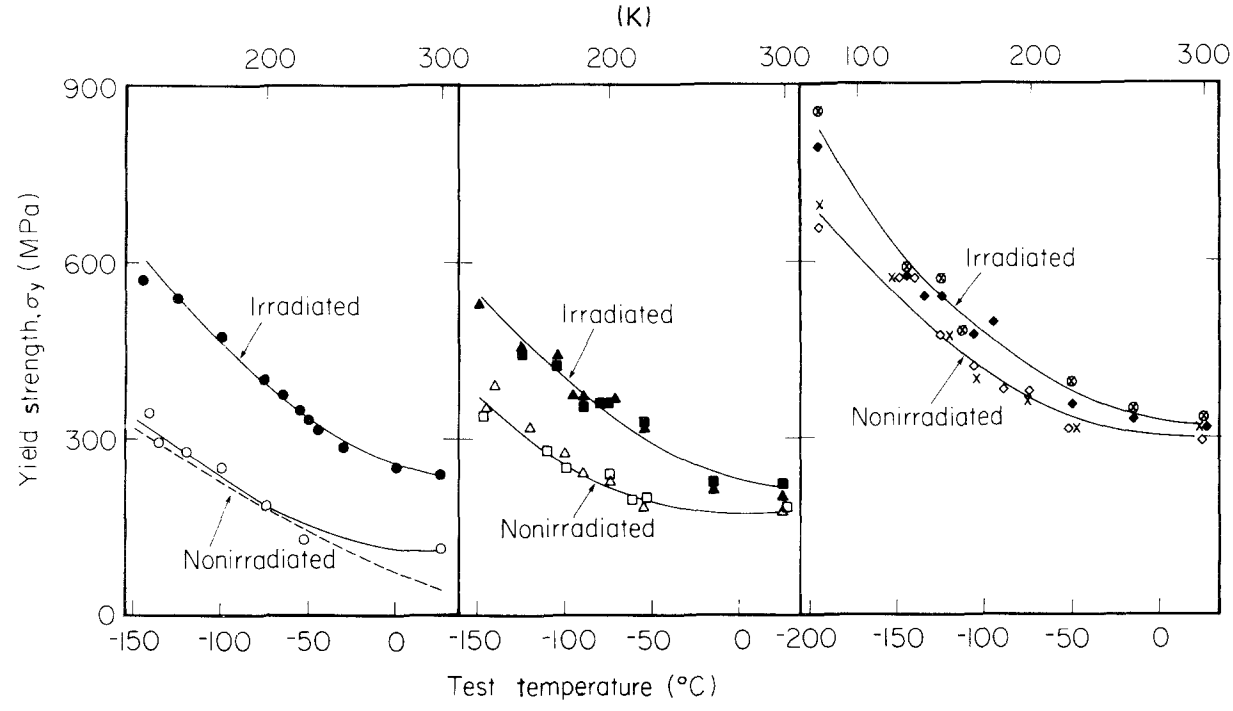

Figure 8 Effect of neutron irradiation on yield strength in various iron alloys: (○, ●) I, Copper-doped, (– – –) pure iron; (△, ▲) II, phosphorus-doped; (□, ■) III, P–Cu-doped; (◇, ◆) IV, P–C-doped; (×, ⊗) V, P–Cu–C-doped alloys.

TABLE I Effect of neutron irradiation on J_{Ic} estimated from TD or SP specimen test of 2.25 Cr–1 Mo steel and copper-doped iron alloy

	δ_f	ε_{qf}	Estimated J_{Ic} (kJ m^{-2})	Valid J_{Ic} (kJ m^{-2})
2.25 Cr–1 Mo steel (TD test)				
Nonirradiated	0.78	0.85	180	245
Irradiated	0.68	0.67	117	148
Copper-doped iron alloy (SP test)				
Nonirradiated	2.07	1.38	363	–
Irradiated	1.85	1.14	280	–

The presence of copper and/or phosphorus is known to promote hardening due to the formation of copper- and/or phosphorus-rich precipitates induced during irradiation in ferritic alloys. Moreover, because the dynamic interaction between solute and defect fluxes occurs during high-temperature irradiation, it is possible that the intergranular solute segregation giving rise to embrittlement is facilitated by neutron irradiation. Therefore, combined effects of hardening and intergranular solute segregation induced by neutron irradiation (9.4×10^{22} neutrons m^{-2} at 668 K, $E > 0.1$ MeV) on embrittlement have been studied in several iron-base alloys containing residual sulphur and doped with phosphorus, copper and/or carbon using the SP testing method and scanning Auger microscopy [9, 20].

Fig. 8 shows the effect of irradiation on the yield strength in various iron alloys [9]. The copper- and/or phosphorus-doped alloys exhibited a greater effect of irradiation on hardening than the carbon-containing alloys. By analysing the temperature dependence of the difference in the yield strength between the non-irradiated and irradiated alloys, it was found that neutron irradiation-induced hardening is attributed mainly to the formation of precipitates and partly to that of defect clusters.

The irradiation effect on the DBTT obtained from the SP test on the various iron specimens is shown in Fig. 9 [9]. As mentioned before, the DBTT shift is expected to be amplified further in the CVN test. The neutron irradiation remarkably increased the DBTT in the copper-doped alloy. The DBTT in the P–Cu-doped alloy was slightly increased by irradiation and conversely it was decreased in the phosphorus- and/or carbon-doped alloys. The effect of irradiation on the DBTT shift is not highly correlated with that on hardening. Intergranular and transgranular fracture occurred in the alloys without and with carbon, respectively. The fracture mode was not affected by the neutron irradiation. Scanning Auger microscopy analyses on the fracture surface showed that while the neutron irradiation increased sulphur segregation in the copper-doped alloy, it decreased sulphur segregation and increased phosphorus segregation in the alloys containing phosphorus [20]. The intergranular segregation of sulphur and phosphorus during irradiation was found to be a nonequilibrium process. Both the increase in sulphur segregation and the strong hardening effect contribute to the great embrittlement effect for the copper-doped alloy. However, in the phosphorus-containing alloy, the intergranular weakening induced by the enrichment of phosphorus segregation is mitigated by the reduction in sulphur segregation giving rise to the toughening effect.

Recently, the effect of neutron irradiation (3.2×10^{23} neutrons m^{-2} at 638 K) on J_{Ic} has been investigated in 2.25 Cr–1 Mo steel using the CT and TD specimen tests [10]. In Table I, the value of J_{Ic} estimated from δ_f is compared with the valid value from the

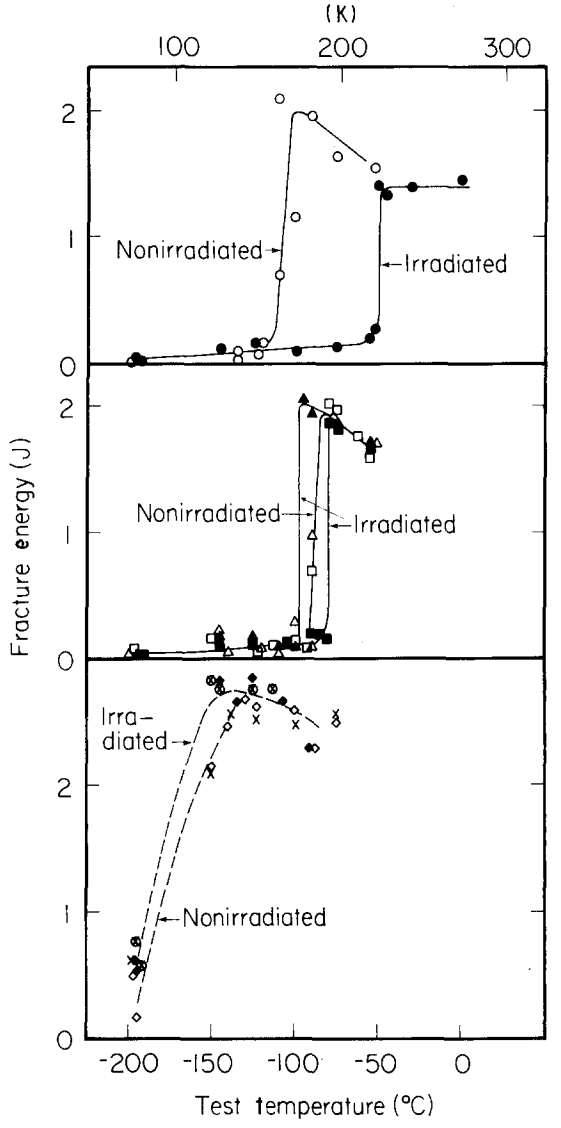

Figure 9 Effect of neutron irradiation on DBTT in various iron alloys: (○, ●) I, Copper-doped; (△, ▲) II, phosphorus-doped; (□, ■) III, P–Cu-doped; (◇, ◆) IV, (×, ⊗) P–C-doped V, P–Cu–C-doped alloys. (○, △, □, ◇, ×) Nonirradiated, (●, ▲, ■, ◆, ⊗) irradiated.

CT test. The estimated value of J_{Ic} is about 20%–25% smaller than the valid value for the nonirradiated and irradiated alloys. The underestimate of J_{Ic} from the TD tests is attributed to the data scattering of the ε_q versus δ/t_0 relationship (Fig. 4). Nonetheless, the degree of neutron irradiation-induced embrittlement found in the TD test exhibited a similar tendency to that in the CT test (40% reduction). Table I also shows an estimate of the irradiation effect on J_{Ic} in the copper-doped alloy from the previously shown SP test result. It is evident that the copper-doped iron alloy showed a weaker embrittlement effect than the 2.25 Cr–1 Mo steel partly because of the lower fluence and higher temperature of neutron irradiation.

6. Conclusion

The recent progress on the development of miniaturized SP and TD testing methods is reported. The yield strength, the ductility and J_{Ic} were estimated by analysing the deformation and fracture behaviour in the SP and TD tests. The DBTT behaviour was clearly observed in the SP and TD tests. A linear correlation between $(DBTT)_{SP}$ and $(DBTT)_{CVN}$ has been established theoretically and experimentally. The effect of neutron irradiation on hardening, DBTT and J_{Ic} has been investigated in various materials using the miniaturized testing technique. It has been shown that its application in evaluating irradiated materials is promising.

Acknowledgements

Ames Laboratory is operated for the US Department of Energy by Iowa State University under contract no. W-7405-ENG-82. This work was supported by the Office of Basic Energy Sciences, Division of Materials Sciences.

References

1. N. H. PACKAN, R. E. STOLLER and A. S. KUMAR (eds), "Effects of Radiation on Materials", ASTM STP 1046 (American Society for Testing and Materials, Philadelphia, 1990).
2. R. VISWANATHAN and B. S. BRUEMMER, *Trans. ASME, J. Engng Mater. Tech.* **107** (1985) 316.
3. G. E. LUCAS, *Metall. Trans.* **21A** (1990) 1105.
4. X. MAO, T. SHOJI and H. TAKAHASHI, *J. Test. Eval.* **15** (1987) 30.
5. X. MAO and H. TAKAHASHI, *J. Nucl. Mater.* **150** (1987) 42.
6. S. TAKAYAMA, T. OGURA, S. FU and C. J. McMAHON Jr, *Metall. Trans.* **11A** (1980) 1513.
7. J. KAMEDA and C. J. McMAHON Jr, *ibid.* **11A** (1980) 91.
8. Y. LU, T. SHOJI and H. TAKAHASHI, *J. Jpn Soc. Mech. Engng* **53** (1987) 1150.
9. J. KAMEDA and X. MAO, *Mater. Sci. Engng* **A112** (1989) 143.
10. X. MAO, H. TAKAHASHI and T. KODAIRA, *Trans. ASME J. Engng Mater. Tech.*, in press.
11. R. VISWANATHAN, private communication, 1989.
12. H. TAKAHASHI, M. A. KHAN and M. SUZUKI, *J. Test. Eval.* **8** (1980) 63.
13. J. M. BAIK, J. KAMEDA and O. BUCK, *Scripta Metall.* **17** (1983) 1443.
14. J. M. BAIK, J. KAMEDA and O. BUCK, in "The Use of Small-Scale Specimens for Testing Irradiated Materials", edited by W. R. Corwin and G. E. Lucas, ASTM STP 888 (American Society for Testing and Materials, Philadelphia, 1986) p. 92.
15. M. P. MANAHAN, A. S. ARGON and O. K. HARLING, *J. Nucl. Mater.* **103–104** (1981) 1545.
16. M. R. BAYOUMI and M. N. BASSIM, *Int. J. Fract.* **23** (1983) 71.
17. T. MISAWA, T. ADACHI, M. SAITO and Y. HAMAGUCHI, *J. Nucl. Mater.* **150** (1987) 194.
18. J. KAMEDA, *Acta Metall.* **34** (1986) 2391.
19. J. KAMEDA and O. BUCK, *Mater. Sci. Engng* **83** (1986) 29.
20. J. KAMEDA and A. J. BEVOLO, *Acta Metall.* **37** (1989) 3283.

Received 17 October 1990
and accepted 25 March 1991